ORIGINAL PAPER

Brain tumor findings in patient with a novel cascaded function

R. Remya[1] · S. Murugan[2] · K. Parimala Geetha[3]

Abstract

To evaluate the Magnetic Resonance Imaging finding able to predict the result in patients with a brain tumor. This paper included different patient images with tumors from the BRATS dataset. In this work, a novel strategy is acquainted with image segmentation to bring up the tumor region. At first, it undergoes filtering activity by different filtering strategies and the performance is analyzed. Among that upgraded Discrete Wavelet Transform (DWT) filtering procedure functions admirably. At that point, image segmentation is implemented by novel methodology as a series of exponential functions, where the definite tumor area is pointed out. The exactness of the portioned yield is computed by different performance measures. The enhanced Discrete Wavelet Transform (DWT) filtering procedure provides an improved exactness of 40.44% and 19.70% for PSNR (Peak Signal to Noise Ratio) measure even in the presence of Gaussian and Rican noise than Berkeley Wavelet Transform approach. In segmentation, the proposed method holds greater accuracy in terms of the performance metrics such as Jaccard and Dice. The exact identification of the abnormal area from the abnormal scan image was made by this approach and broadening their life time.

Keywords Magnetic resonance imaging · Threshold · Exponential function · Brain tumor

1 Introduction

Brain tumor growth is one of them as late-developing illnesses for both grown-ups and matured individuals. Such sicknesses have to be distinguished by the Experts toward complete finding out regarding the patient through analyzing. CT (Computerized Tomography) gives detailed data of the patient. Sometimes, they might inject some drugs to recognize the tissues in the frontal cortex. Regardless, in light of radiations, it may incite dangerously to individuals. Nowadays, doctors learn about MR (Magnetic Resonance) imaging; since it doesn't need any radiation. Here too, a drug has imbued to update the tissues of the cerebrum [1]. Rekha et al. [2] stated that the impact of noise such as Gaussian noise has to be removed by double-density dual-tree wavelet transform. Also, it uses the Fast Bilateral Filter (FBF) and double-density wavelets to improve its quality. Lahmiri et al.

stated that [3], an iterative wiener filtering has been utilized to reduce the noisy effect. First Weiner filter output has to be the input to the next Wiener filter. Likewise, the process continues; till it reaches the maximum energy. The work reported in [4]; states the necessity of Discrete Wavelet Transform (DWT) when contrasted with the Discrete Cosine Transform and Fourier Transform. Also, it states that during computation, no prior information regarding the noisy information has needed. The attained result has a noise-free output; also, the peak signal-to-noise gets improved. Mohan et al. [5] stated that it uses both wiener and median filters to attain noise-free images. It can replace noise such as spotted noise, Poisson noise, and salt and pepper noise. Lahmiri and Boukadoum [6] explained that variegated noise such as Gaussian, Poisson, Salt and Pepper, and speckle noise reduced from the images by utilizing the filtering approach with a high PSNR value. For filtering, initially, the Wiener filter is processed, and its outcome has to be processed further by Partial Differential Equation (PDE) to preserve the edge information. Verma et al. [7] reported that the Additive White Gaussian Noise (AWGN) has to be removed by the combination of two methodologies, such as Wavelet and Empirical mode decomposition (EMD). Tian et al. [8] proposed that the presence of Gaussian noise has to be identified by discriminative learning

✉ R. Remya
remiamernath@gmail.com

1 Arunachala College of Engineering for Women, Nagercoil, India

2 Francis Xavier Engineering College, Tirunelveli, India

3 Nalla Malla Reddy Engineering College, Hyderabad, India

based on deep learning. Also, the real noise presence has to be analyzed by the optimization models based on deep learning. While utilizing the Gaussian filter [9], it assigns the weight based on the Gaussian function. In Discrete Wavelet Transform (DWT) filtering, the input image has decomposed into variegated coefficients [10]. Its improved version has seen in [11]. Pursued by this Berkeley Wavelet Transform (BWT) stated in [12] that, it has the phase filters in odd and even numbers.

After filtering, segmentation has been carried, which has explained below. The segmentation operation has to be improved by the new deep neural network. Such an algorithm improves the super-resolution of the image, which has been named the S2 Net [13]. The performance of brain tumor detection has to be enhanced by approaches such as Hidden Markov Model and Threshold approaches to reduce the difficulty in identifying the infected region. And it has been recognized as the hybrid approach [14]. After the pre-processing approach, segmentation has been done with a K-means clustering algorithm to extract the neighboring tissues. Afterward, Hierarchical Centroid Shape Descriptor has utilized to segment out the tumor region alone [15].

Weng and Zu stated in their work that; by increasing the size of the kernel in the convolutional layer. Afterward, it concatenates all the features extracted by kernels. Also, INet utilizes two overlapping max-pooling layers to extract the sharp features [16] Ji et al. [17] stated that by preserving the edge content, the Convolutional Neural Network (CNN) utilizes a Holistically nested Edge Detection (HED) layer. Also, it overcomes the drawback of spatial consistency. Han et al. [18] stated that the Dense Convolution Unit (DCU) has to be utilized by pixel classification, and it is better than the standard CNN. Hussain et al. [19] proposed the Contextual level set method. Instead of considering the low features alone, contextual features have been considering to earn the contextual features. It has the advantage that it can withstand any inhomogeneity in intensity. A Holder exponent [20] has to use for efficient segmentation. The holder exponent has to extract from the Gabor wavelet.

The significant factors to consider in this paper sorts below.

i. The evaluation has to make on BRATS 2015 dataset [21].
ii. An enhanced Discrete Wavelet Transform (DWT) filtering algorithm has to utilize as a pre-processing step.
iii. A cascaded exponential function has to evaluate for image segmentation.
iv. Then Segmentation accuracy has been carried to evaluate the performance, and it has to compare against the state-of-the approaches.

The rest of the paper outlines as:

Section II explains the proposed evaluation, section III brings the experimental outcomes and in section IV, it winds up our novel approach.

2 Methods

In the proposed work, the processing is done in three stages, such as image filtering, image segmentation, and performance evaluation. In this section, an enhanced DWT filtering is detailed here.

2.1 Enhanced discrete wavelet transform (DWT) filtering

The enhanced DWT filtering technique adopted in [11] has to be used even in the presence of noise such as Rician noise, Poisson, Gaussian noise, and salt and pepper noise. There it utilizes soft thresholding; such thresholding operation has to do with the support of threshold value, which has to compute by using Eq. (1) as

$$Thre = \frac{1}{ag} \frac{\sum_{b=1}^{a} \sum_{h=1}^{g} i_{bh}^{3}}{\sum_{b=1}^{a} \sum_{h=1}^{g} i_{bh}} \tag{1}$$

Here the value of a and g depends on the row and column size of the image i. Also, 'i' represents the DWT transformed image. By utilizing the 'Thre' value, the soft thresholding operation is done. Its evaluation is denoted as

$$Sof = \frac{1}{1 + X_m^2} sign(E)(|E| - Thre) \tag{2}$$

sign(E) represents the signum function, it generates the output as '1'; if the value of E is regarded as a larger value than '0', the output is regarded as a larger than '0' and the output is '-1',it E is equivalent to '0'. Finally, the 'Xm' value is evaluated as

$$X_m = \frac{\max(E) + \min(E)}{2} \tag{3}$$

Once the threshold calculation is over; by utilizing the threshold value, IDWT is said to be performed and it is denoted as 'D'.

2.2 Image segmentation

The inverse discrete wavelet transformed output has regarded as the filtered response. For that filtered output, a segmentation operation has been done. Such a task is performed in our work by a novel approach named as s series of functions. The

performance has improved when contrasted with the previous approaches, which incorporate Fuzzy clustering, watermarking, and IVIFs algorithms. This approach plays a vital role in detecting the presence of brain tumors at their early stage. The proposed approach evaluation has been given in the form of an algorithm as follows,

Step 1: The filtered image, D has been utilized as the input for segmentation.

Step 2: Afterward evaluate the median value 'C'.

Step 3: Using that median value, determine the parameter 'p' utilizing Eq. (4)

Step 4: With the parameter 'p', estimate the function 'S' as in Eq. (5).

Step 5: The function 'S' evaluation relies upon both the filtered image and the parameter 'p'.

Step 6: The function 'S' computation is completely relies on the cascaded exponential function as in condition (6).

In the current work, initially it calculates the median of the portioned picture. The median computation is done by at first sorting all the pixel esteems among the areas in an increasing order looks at to the middle pixel. Furthermore, it contains an odd number of pixel values. By then, the middle pixel is considered as the median value. In case, it contains more number of pixels, by then the median value is figured by registering the average of the middle two pixels.

Such a median calculations denoted by the parameter called 'C'. By utilizing this, the estimation of the parameter 'p' has made by the equation as,

$$p = \frac{\sqrt{C}}{2} \tag{4}$$

By utilizing this, the segmentation has been done to extract the tumor region as in Eq. (5)

$$S = f(F, p) \tag{5}$$

Here, 'F' represents the filtered image. The above equation shows that the function 'F' and the parameter 'p'. The expanded version is given as

$$f(F, p) = \frac{\exp(A)^4}{4!} + \frac{\exp(A)^3}{3!} - \frac{\exp(A)^2}{2!} + \frac{\exp(A)}{1!} \tag{6}$$

,

where A=F+p. Using the above equation, we can observe there is series of exponential function, using that we can reserve more details compared to the state-of-the-art approaches.

2.3 Performance evaluation

The performance estimation of the current work has been done and compared against the other algorithms by utiliz-
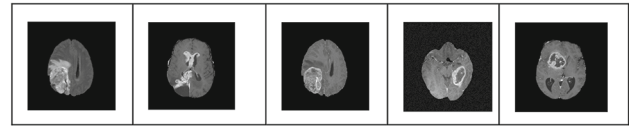

Fig. 1 Input image

ing the parameters such as PSNR, SSIM, NAE, Jaccard, and Dice. The segmented result from the proposed algorithm has to evaluate against the ground truth. The proposed automatic segmentation result has to compare with the ground truth images available in the BRATS dataset [21]. Figure 1 shows the input images utilized for usage. In the first step, by using the input images perform image filtering as a pre-processing step. After filtering, segmentation has to carry out to point the tumor locale precisely, and it has explained in the second part. In the third part, segmentation accuracy has to assess. Based upon this assessment, we finish up the utilization of specific parameters for the segmentation.

This section has to sort as:

The exactness of the segmented result is estimated by the variegated evaluation measures and characterized in the area "Performance metric definition". In the section "filtering simulated results" we clarify the simulation results of filtering activity, in the section "Segmentation simulated results" the implementation details of segmentation have been illustrated. For execution, MATLAB 2016a has to utilize for programming with windows 10 OS.

2.4 Metric definition

Usually, the performance evaluation has made between the yielded one and the reference image. Here the execution has been made between those images with the support of several performance measures. It is said to be utilized both filtering and segmentation uniquely. For filtering, both PSNR and SSIM were used. Likewise for segmentation, Dice, Jaccard, VOE, and NAE have been used to evaluate their exactness; such a comparison has to perform among the segmented output as well as ground truth images.

2.5 PSNR (Peak signal to noise ratio)

To measure the accuracy of the reconstruction, PSNR has been regarded as one of the widely used performance measures. It has been given in terms of dB as

$$PSNR(D, I) = 10 \log \frac{255^2}{MSE(D, I)} \tag{7}$$

Highest PSNR value points out that the clarity of image is higher. Here D and I represent the filtered and test images respectively.

2.6 SSIM (Structural similarity index measure)

SSIM metric evaluation has based on statistical values between the test and filtered image [22].

$$SSIM(D, I) = \frac{(2M_D M_I + C_a)(2V_{DI} + C_b)}{(M_D^2 + M_I^2 + C_a)(V_D^2 + V_I^2 + C_b)} \quad (8)$$

,

where C_a and C_b are constants, M_D and M_I be the mean of the filtered and the test images respectively; and the term V represents the variance.

2.7 NAE (Normalized absolute error)

It has been represented algebraically as in Eq. (11),

$$NAE = \frac{\sum\limits_{s=1}^{S'} \sum\limits_{g=1}^{G'} |S_{sg} - R_{sg}|}{\sum\limits_{s=1}^{S'} \sum\limits_{g=1}^{G'} S_{sg}} \quad (9)$$

S_{sg} and R_{sg} speak about the segmented and filtered image in the pixel location (s, g). Here, S and R represents the segmented and ground truth images, respectively. Also S' and G' shows the row and column size of the image. Furthermore, s and g represents the filtered and test image at location (s, g). The highest value of NAE points out that the image clarity is low [23].

2.7.1 Jaccard (JA)

Jaccard similarity index is evaluated among segmented output and ground truth images as the ratio of its intersection and union. It is expressed as in Eq. (12)

$$JA = \frac{S \cap R}{S \cup R} \quad (10)$$

Here, S and R speak about the segmented and the ground truth images respectively.

2.7.2 VOE (Volumetric overlap error)

It is computed with the help of the Jaccard similarity index. The VOE value is evaluated as in Eq. (13),

$$VOE = 1 - JA = 1 - \frac{S \cap R}{S \cup R} \quad (11)$$

If the VOE value is '1', it shows the low similarity among the segmented and ground truth images. If the VOE value is '0', it indicates that a high similarity among the images.

2.7.3 Dice (DI)

It is an important parameter and it is most widely used for medical image segmentation accuracy calculation. It is defined by the ratio of normalizing the intersection between the segmented as well as ground truth images and their averages [24]. It is expressed as,

$$DICE = \frac{|S \cap R|}{\frac{1}{2}(|S| + |R|)} = \frac{2|S \cap R|}{|S| + |R|} \quad (12)$$

If the value is nearer to '0', it shows the low similarity among the images. If the value is nearer to '1', it indicates that a high similarity among the images.

3 Results

3.1 Image filtering simulated results

The filtering execution examination is made on the PSNR and SSIM performance measures. Table 1 depicts that the examined result of enhanced DWT is having the greater outcome by 40.4399% for the PSNR value as an average than BWT; while Gaussian noise is said to be included. Likely, the execution of enhanced DWT was raised by 39.42% for SSIM as an average than BWT. Also while including Rician noise; enhanced DWT was 19.6997% higher than the BWT method. Furthermore, the enhanced DWT method attains 35.4114% than the BWT approach, while considering the Poisson noise. Here too SSIM worth is raised by 4.925% than BWT approach. Depending upon the above results, we have chosen that enhanced DWT filtering for filtering.

3.2 Segmentation simulated results

The output attained after filtering to be utilized for the segmentation operation. The proposed work ran successfully with all the images. The performance evaluation is made among the segmented output and the ground truth images. Furthermore, the comparison is made by utilizing the metrics such as Dice, Jaccard, VOE, and NAE. The novel methodology results and the state-of-the-art results are shown in Fig. 2. Here, the proposed results show that the accurate results were obtained for our proposed work is improved than other works such as Fuzzy C-Means (FCM), interval-valued intuitionistic fuzzy sets (IVIFSs) [25], watermarking and marker-based watermarking. Also from Fig. 2, we can justify that the current work generates a result with improved performance than the other similar works, whereas it replaces the unwanted portions which were present in the previous works. Also, the output resembles the ground truth images. Furthermore, it shows that watermarking results show the unnecessary seg-

Table 1 Filtering performance evaluation is made; when Gaussian, Rician and Poisson noise is added

Images	Gaussian noise			
	PSNR		SSIM	
	BWT	Enhanced DWT	BWT	Enhanced DWT
Image 1	29.452	49.0410	0.608	0.9973
Image 2	28.509	47.9742	0.607	0.9972
Image 3	28.830	48.3680	0.602	0.9972
Image 4	27.888	47.2744	0.597	0.9971
Image 5	28.488	47.7287	0.604	0.9971
Average	28.634	48.7287	0.604	0.9972
Images	Rician noise			
	PSNR		SSIM	
	BWT	Enhanced DWT	BWT	Enhanced DWT
Image 1	34.607	52.4799	0.9194	0.9990
Image 2	32.036	50.2127	0.9095	0.9989
Image 3	32.598	20.8997	0.9052	0.9988
Image 4	30.763	49.1958	0.8885	0.9986
Image 5	31.988	49.8474	0.8993	0.9987
Average	32.398	40.3471	0.9044	0.9988
Images	Poisson noise			
	PSNR		SSIM	
	BWT	Enhanced DWT	BWT	Enhanced DWT
Image 1	35.012	52.5570	0.956	0.9991
Image 2	32.300	50.2803	0.946	0.9990
Image 3	32.859	50.9758	0.940	0.9989
Image 4	30.905	49.2401	0.921	0.9987
Image 5	32.363	49.9948	0.933	0.9988
Average	32.688	50.6096	0.939	0.9989

Fig. 2 First row shows the watermarking output, second row depicts the marker-based watermarking result, third row demonstrates the FCM output, fourth row shows the IVIFSs results and fifth row shows the our proposed results

Fig. 3 Ground truth images

mented area. In marker-based watermarking approach, edge portions were not identified properly. Furthermore, the FCM result depicts that nearer to the edge region, the accuracy is high, but the inaccurate results may occur outside the tumor region. IVIFSs give the result of higher accuracy than the FCM approach, but also there will be some degradation in accuracy due to noise. It was controlled by our proposed approach. The ground truth images are given in Fig. 3, and it is utilized for outcome comparison to demonstrate its accuracy.

Also, the segmentation performance has been evaluated by the metrics such as dice, Jaccard, VOE, and NAE. The segmentation performance examination is made among the segmented output and the ground truth images. From Table 2, we can refer that the current work holds better results in all the cases. It demonstrates that the accuracy comparison
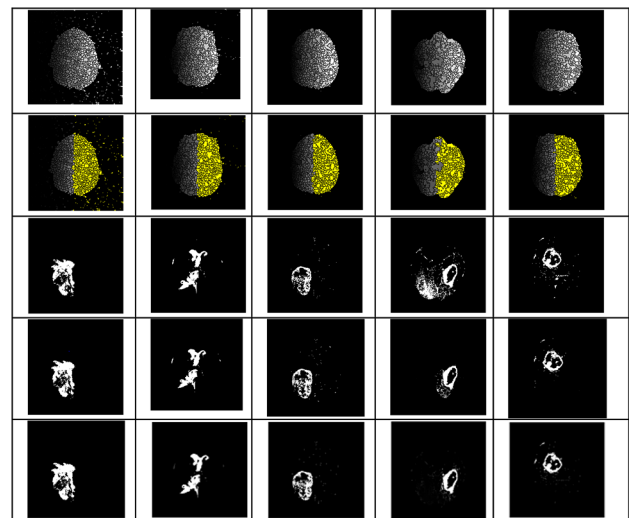
is based on the performance evaluation metrics such as dice, Jaccard, NAE, and VOE.

When evaluating the performance, the Dice accuracy of the current algorithm was raised by 99.99%, 90.92%, 13.65%, and 5.43% than watermarking, marker-based watermarking, FCM and IVIFSs respectively. For Jaccard; the accuracy of the proposed algorithm was increased by 96.36%, 91.96%, 11.01%, and 2.34% than previous segmentation approaches respectively. Similarly, for VOE performance measures the exactness was improved as 48.05%, 46.72%, 8.03%, and 5.72% for the other previous segmentation approaches respectively is shown in Table 2. Furthermore, the NAE parameter also improved in our proposed approach.

Also, the comparison is done without any noise. The obtained result has given in Fig. 4. Here too, our current work holds gained results than the other similar works. It depicts that; our current approach was improved for the Dice metric by 99.99%, 43.7%, 99.07%, and 15.67% when compared with other previous segmentation approaches. Moreover, for the Jaccard metric, the accuracy of the current method was gained by 96.38%, 59.11%, 12.22%, and 9.91% than other segmentation methodologies respectively. Likewise, for VOE performance measures the exactness was reduced as 51.07%, 45.39%, 12.23%, and 6.7% for watermarking,

Table 2 Segmentation accuracy comparison in the presence of Gaussian noise with the variegated performance parameters

| Methods images | DICE | | | | |
	water marking	Marker-based water marking	FCM	IVIFSs	Proposed
Image 1	5.89e-6	0.0009	0.521	0.620	0.8085
Image 2	9.39e-6	0.1043	0.823	0.830	0.8335
Image 3	5.76e-6	0	0.634	0.654	0.6660
Image 4	2.31e-6	0.1416	0.445	0.461	0.4639
Image 5	5.40e-6	0.0834	0.716	0.805	0.8647
Average	5.75e-6	0.0660	0.628	0.673	0.7273
Method images	Jaccard				
	water marking	Marker-based water marking	FCM	IVIFSs	Proposed
Image 1	0.0222	4.62e-4	0.352	0.389	0.3638
Image 2	0.0327	0.550	0.699	0.725	0.7485
Image 3	0.0180	0.0330	0.464	0.483	0.4993
Image 4	0.0075	0.0762	0.286	0.314	0.3225
Image 5	0.0181	0.0485	0.557	0.677	0.6977
Average	0.0193	0.0426	0.472	0.518	0.5304
Method images	VOE				
	water marking	Marker-based water marking	FCM	IVIFSs	Proposed
Image 1	0.9798	0.9995	0.647	0.6309	0.5362
Image 2	0.9673	0.9450	0.329	0.3274	0.3215
Image 3	0.9820	0.9560	0.535	0.5083	0.5007
Image 4	0.9925	0.9238	0.739	0.7480	0.7218
Image 5	0.9819	0.9565	0.521	0.4874	0.4672
Average	0.9807	0.9562	0.554	0.5404	0.5095
Method Images	NAE				
	water marking	Marker-based water marking	FCM	IVIFSs	Proposed
Image 1	2.23e + 5	1.3106	377.85	1.252	0.8970
Image 2	1.27e + 5	2.5208	0.3310	2.002	0.0652
Image 3	2.02e + 5	4.0473	0.6585	0.602	0.5465
Image 4	4.88e + 5	7.0756	3.3953	1.568	0.1299
Image 5	2.18e + 5	3.9477	169.06	55.82	0.5791
Average	2.52e + 5	3.7804	110.25	12.25	0.4435

Fig. 4 Segmentation results without any noise for the proposed method

The outcome show that the segmented image obtained is more accurate, compared to the other similar methods. All the results obtained from the current method were obtained with a good satisfactory level.

4 Conclusion

In the current work, the author proposed a computerized segmentation approach. The MATLAB simulation is done on different images of the same size in the BRATS dataset. The image filtering utilizes an enhanced DWT to create noise-free images; which expels an undesirable distortion at an average of 35.41% and 4.93% for PSNR and SSIM similarity met-

marker-based watermarking, FCM, and IVIFSs segmentation, respectively, is given in Table 3.

Likewise, the NAE metric has been reduced in the current work. Since NAE value should be as low as possible to shows the better accuracy. Table 3 depicts that the current work has lower value than watermarking, marker-based watermarking, FCM, and IVIFSs techniques, respectively.

Table 3 Segmentation accuracy comparison without any noise using the variegated performance parameters

| Methods Images | DICE | | | | |
	water marking	Marker-based water marking	FCM	IVIFSs	Proposed
Image 1	0.0023	0.2882	0.004	0.5311	0.5685
Image 2	0.0022	0.1774	0.008	0.8082	0.8124
Image 3	0.0030	0.3597	0.006	0.2960	0.6847
Image 4	0.1420	0.1420	0.003	0.4093	0.4712
Image 5	5.65e-6	0.0755	0.007	0.6765	0.6895
Average	0.0299	0.2086	0.006	0.5442	0.6453
Method Images	Jaccard				
	water marking	Marker-based water marking	FCM	IVIFSs	Proposed
Image 1	0.0177	0.6184	0.349	0.3522	0.3613
Image 2	0.0338	0.0973	0.682	0.6770	0.7485
Image 3	0.0171	0.2193	0.444	0.4897	0.5041
Image 4	0.0072	0.0764	0.311	0.2842	0.2573
Image 5	0.0173	0.0393	0.467	0.5112	0.6977
Average	0.0186	0.2101	0.451	0.4629	0.5138
Method Images	VOE				
	water marking	Marker-based water marking	FCM	IVIFSs	Proposed
Image 1	0.9823	0.8316	0.652	0.6387	0.5360
Image 2	0.9662	0.9027	0.317	0.3227	0.2815
Image 3	0.9829	0.7807	0.556	0.5241	0.4959
Image 4	0.9928	0.9238	0.689	0.6612	0.6200
Image 5	0.9819	0.9565	0.521	0.4263	0.4672
Average	0.9812	0.8791	0.547	0.5146	0.4801
Method Images	NAE				
	water marking	Marker-based water marking	FCM	IVIFSs	Proposed
Image 1	530.1484	1.9987	361.26	55.82	1.2475
Image 2	617.2350	3.2292	178.80	29.37	0.8020
Image 3	393.5524	1.3446	0.6585	0.632	0.6174
Image 4	1.662e + 3	6.9041	703.55	2.739	1.1299
Image 5	2.203e + 5	4.9729	156.41	0.551	0.4321
Average	4.470e + 4	3.6599	280.14	17.82	0.8458

rics than BWT filtering. Following this, image segmentation is done as it depends on the series of the exponential function. On the way that all images having the brain tumor is distinguished. The primary advantage is that for early analysis, this methodology functions admirably. Here, in work, it delivers an average improvement of 49.56%, 46.06%, 10.13%, and 6.21% for VOE metric when contrasted with watermarking; marker-based watermarking; FCM; and IVIFSs segmentation respectively. In general, our calculation results depict that our technique is prevalent even in the presence or absence of noise. Likewise, it saves the detail which was considered as a good compromise. In this work, the edge details have to preserve more precisely.

It aims to extend the work toward the characterization of the images based on the tumor size, shape, texture, edge details, etc. By utilizing those features, automated classification to be made at its grade level.

References

1. Charalampaki, C., et al.: Neurosurgery. Neuro Oncology. **16**(1), 105–108 (2014)
2. Rekha, H, Samundiswary, P.: Double density wavelet with fast bilateral filter based image denoising for WMSN. In: 9th International Conference on Advanced Computing ICoAC 2017. 315–319 (2018)

3. Lahmiri, S.: An iterative denoising system based on Wiener filtering with application to biomedical images. Optics and Laser Tech. **90**, 128–132 (2017)

4. Vimala, C., Aruna Priya, P., Subramani, C.: Wavelet transform approach for image processing – a research motivation for engineering graduates. Int J Electr Eng Educ **58**(2), 373–384 (2021)

5. Mohan Sai S, Muppa S, Mona Teja K, Natrajan P.: Advanced image processing techniques based model for brain tumour detection. In: 4th International Conference on Computing Communication and Automation, ICCCA 2018, 1–6 (2018)

6. S. Lahmiri and M. Boukadoum.: A comparison of four PDE-spatial denoising systems for molecular images. In: IEEE 8th Latin American Symposium on Circuits and Systems (LASCAS), 1–4, (2017)

7. . Verma, A., Pratik., Pradhan, G.: Electrocardiogram denoising using Wavelet decomposition and EMD domain filtering, 2016 IEEE Region 10 Conference (TENCON), 2185–2189 (2016)

8. Tian, C., Fei, L., Zheng, W., Xu, Y., Zuo, W., Lin, C.: Deep learning on image denoising: an overview. Neural Netw. **131**, 251–275 (2020)

9. Xie, Q.-L.: Adaptive Gaussian smoothing filter for image denoising. J comput eng appl **45**(16), 182–184 (2009)

10. Chung- Wei Liang and Po-Yueh Chen: DWT based text localization. Int J appl sci eng **2**, 105–116 (2004)

11. Remya. R, Geetha. K. Parimala and Sundaravadivelu. S.: Enhanced DWT filtering technique for brain tumor detection. IETE J Res. https://doi.org/10.1080/03772063.2019.1656555 (2019)

12. Ben Willmore, Ryan J Prenger and Michael C-K Wu and Jack L Gallant.: The Berkeley Wavelet transform: a biologically-inspired orthogonal wavelet transforms, neural computation, 1–5 https://www.researchgate.net/publication/5657666 (2015)

13. S. Lei, Z. Shi, X. Wu, B. Pan, X. Xu and H. Hao.: Simultaneous super-resolution and segmentation for remote sensing images IGARSS. In: IEEE International Geoscience and Remote Sensing Symposium, 3121–3124. https://doi.org/10.1109/IGARSS.2019.8900402 (2019)

14. H. S. Abdulbaqi, M. Zubir Mat, A. F. Omar, I. S. Bin Mustafa and L. K. Abood.: Detecting brain tumor in magnetic resonance images using hidden markov random fields and threshold techniques. In: IEEE Student Conference on Research and Development. https://doi.org/10.1109/SCORED.2014.7072963 (2014)

15. Raj, C.P.S, Shreeja, R.: Automatic brain tumor tissue detection in T-1 weighted MRI. In: International Conference on Innovations in Information, Embedded and Communication Systems (ICIIECS), 1–4 (2017)

16. Weng, W., Zhu, X.: INet: convolutional networks for biomedical image segmentation. IEEE Access **9**, 16591–16603 (2021)

17. Ji, J., Lu, X., Luo, M., Yin, M., Miao, Q., Liu, X.: Parallel fully convolutional network for semantic segmentation. IEEE Access **9**, 673–682 (2021)

18. Han, C., Duan, Y., Tao, X., Lu, J.: Dense convolutional networks for semantic segmentation. IEEE Access **7**, 43369–43382 (2019)

19. Hussain, S., Xi, X., Ullah, I., Wu, Y., Ren, C., Lianzheng, Z., Tian, C., Yin, Y.: Contextual level-set method for breast tumor segmentation. IEEE Access **8**, 189343–189353 (2020)

20. Palanivel, D.A., Natarajan, Sivakumaran, Gopalakrishnan, Sainarayanan: Retinal vessel segmentation using multifractal characterization. Appl Soft Comput **94**, 106439 (2020)

21. Menze, B.H., et al.: The multimodal brain tumor image segmentation benchmark, (BRATS). IEEE Trans Med Imag **34**(10), 1993–2024 (2015)

22. Wang, Z., Bovik, A.C., Sheikh, H.R., Simoncelli, E.P.: Image quality assessment from error visibility to structural similarity. IEEE Trans. Image Process. **13**(4), 600–612 (2004)

23. Memon, F., Unar, M.A., Menon, Sheeraz: Image quality assessment for performance evaluation of focus measure operators. Mehran Univ Res J Eng Technol **34**(4), 379–386 (2015)

24. Xia, Z., Gan, Y., Xiong, J., Zhao, Q., Chen, J.: Crown segmentation from computed tomography images with metal artifacts. IEEE sign process lett. **23**, 678–682 (2016)

25. Ananthi, V.P., Balasubramaniam, P., Kalaiselvi, T.: A new fuzzy clustering algorithm for the segmentation of brain tumor. Soft. Comput. **20**, 4859–4879 (2015)